ELSEVIER

Chemical Engineering Journal 87 (2002) 135–147

Chemical Engineering Journal

www.elsevier.com/locate/cej

# Quantification, by image analysis, of effect of operational conditions on size and shape of precipitated barium sulphate

B. Bernard-Michel, M.N. Pons*, H. Vivier

*Laboratoire des Sciences du Génie Chimique, CNRS ENSIC-INPL 1, rue Grandville, BP 451, F-54001 Nancy Cedex, France*

Received 12 January 2000; received in revised form 1 December 2000; accepted 18 April 2001

**Abstract**

The size and morphology of precipitated barium sulphate crystals have been quantified by semi-automated image analysis. Using a set of six bi-dimensional shape descriptors and a pseudo-3D parameter and with the help of statistical tools such as principal component analysis and factorial discriminant analysis, it is possible to discriminate the various habits of barite, found in literature or obtained in our experiments under various operational conditions (single or double feed, feed injection position, feed rates) related to macro and micromixing. By examination of sets of at least 80 crystals per sample, the effect of these conditions on the shape and size of barite have been evaluated. 

*Keywords:* Barium sulphate; Precipitation; Morphology; Image analysis; Operational conditions

## 1. Introduction

Barium sulphate or barite, used in the paint and paper industries as well as in oil production, can be extracted from the ground or synthesised by precipitation. Besides its economical interest, it has been largely used as a test product to investigate the effect of various process conditions in precipitation (especially related to mixing) and to develop precipitation models. Its key advantage is that, on the contrary to calcium oxalate, there is no hydrated form.

Gunn and Murthy [1], and Murthy [2] examined the development of the barium sulphate crystal shape in relation with nucleation, diffusion and surface reaction. Crystallisation and agglomeration kinetics were determined by Hostomsky and Jones [3] in a continuous stirred-tank crystalliser. Angerhöfer and Mersmann [4] studied nucleation and growth kinetics from batch precipitation. The effect of additives on crystals morphology for a batch crystalliser were investigated by Kipp et al. [5]. In a similar direction Aoun [6] demonstrated the effect of the nature of counter-ions when sodium, lithium, potassium, caesium, calcium or magnesium salts are used as source of sulphate. Mohanty et al. [7] characterised the crystals produced in a reactor equipped with a mixing tee. Fitchett and Tarbell [8] studied the effect of mixing intensity on size of crystals for a continuous stirred-tank crystalliser. These authors noticed a strong change in the crystal habits depending upon the reagent feed concentration. Meyer et al. [9] studied segregation at pilot scale. Baldyga et al. [10] developed a model describing interactions between mixing of various scales (macro-, meso- and micromixing) coupled with the population balance for crystallisation. Their experiments were carried out in a double feed semi-batch reactor. More recently two mixing scales (macro and micro) were used by Philips et al. [11] in their modelling of single feed semi-batch precipitation of barium sulphate. A rectangular reactor was tested by van Leeuwen et al. [12] who examined in particular the influence of hydrodynamics on crystal size and shape in this new configuration. Pénicot et al. [13] studied the influence of the internal crystalliser geometry and the operational conditions on the solid product quality.

In all these studies, it has been noticed that barium sulphate crystals can present many different habits, even in a given experiment: Baldyga et al. [10] obtained a mixture of crystals presenting two habits in their double-feed semi-batch experiment with inclined feed tubes when Philips et al. [11] presents a SEM photograph with three habits observed by feeding near the surface (single-feed semi-batch). However, except in some occasions where the dimensions of crystals were measured manually on micrographs, the descriptions are qualitative: it is difficult to clearly relate one shape to another, and as noted by Baldyga et al. [10], to explain and predict the morphology of crystals. Furthermore, the crystal size distributions (CSD), on which are based the

* Corresponding author. Tel.: +33-3-83-17-52-77; fax: +33-3-83-17-53-26.
*E-mail address:* marie-noelle.pons@ensic.inpl-nancy.fr (M.N. Pons).

1385-8947/02/$ – see front matter 
PII: S1385-8947(01)00212-1

**Nomenclature**

| | |
|---|---|
| $a$ | coefficient in principal component analysis |
| $C$ | circularity |
| CI | surface concavity index |
| $d$ | distance between jets (m) |
| $D$ | turbine diameter (m) |
| $D_{eq}$ | surface equivalent diameter (μm) |
| $f_i$ | principal component |
| $F_{max}$ | maximal Feret diameter (μm) |
| $F_{min}$ | minimal Feret diameter (μm) |
| INF | influence factor |
| $K_s$ | solubility ($mol^2\,l^{-2}$) |
| $\bar{L}$ | average crystal diameter (μm) |
| $L_p$ | equivalent diameter of platelet particles (μm) |
| $L_{sr}$ | equivalent diameter of sand-roses particles (μm) |
| $m$ | number of descriptors |
| $n$ | number of particles |
| $N$ | stirring speed (rpm) |
| $P$ | Crofton perimeter (μm) |
| $s$ | number of principal components |
| $S$ | silhouette surface ($\mu m^2$) |
| $S_c$ | convex bounding polygon surface ($\mu m^2$) |
| $t_c$ | circulation time (s) |
| $T$ | reactor diameter (m) |
| $V_0$ | initial volume (l) |
| $V_{Ba}$ | added volume of barium chloride solution (l) |
| $V_K$ | added volume of potassium sulphate solution (l) |
| $X_{sr}$ | proportion of sand-roses particles |

*Greek letters*

| | |
|---|---|
| $\alpha$ | significance level |
| $\beta$ | local turbulence level |
| $\varepsilon$ | local energy dissipation rate per unit mass ($W\,kg^{-1}$) |
| $\gamma$ | reactant volume ratio |
| $\nu$ | kinematic viscosity ($m^2\,s^{-1}$) |
| $\sigma$ | supersaturation |
| $\Omega_1$ | robustness |
| $\Omega_2$ | largest concavity index |
| $\tau_w$ | micromixing time (s) |
| $\omega_i$ | number of erosions |
| $\xi$ | simplicity |

kinetics laws and growth rates, are classically determined with laser granulometers and in these devices the particles are generally considered as spheres. On some devices a constant "shape factor" can be selected. Assumptions on shape can affect the veracity of the size distributions [14–16]. A quantitative description of the morphology of a particle population can be proposed nowadays, via image analysis: as the size of a non-spherical particle should be described by a set of lengths, its shape is represented through a set of shape descriptors [17]. This morphological quantification leads to important information on the complex phenomena taking place in precipitation. This approach has been successfully used in the case of calcium oxalate precipitation [18]. The purpose of this contribution is to describe quantitatively the effect of mixing on the shape of barium sulphate crystals and to provide a basis for the quantification of the morphology that could be introduced in models.

## 2. Materials and methods

### 2.1. Experimental

Experiments were carried out in a 2 l stainless steel jacketed rounded-bottom reactor (Fig. 1). A Rushton turbine was used as stirring device. Temperature was controlled at 22 °C by a water bath. The reactor contained initially deionised water ($V_0 = 1.6$ l). Equal volumes of potassium sulphate ($V_K$) and barium chloride ($V_{Ba}$) solutions were added with $V_K = V_0/\gamma$ and $\gamma = 10$. The concentrations were calculated in order to have an overall supersaturation ratio $\sigma$ equal to 190. The supersaturation $\sigma$ is defined as:

$$\sigma = \frac{\lfloor SO_4^{2-} \rfloor \lfloor Ba^{2+} \rfloor}{K_s} - 1$$

where $\lfloor SO_4^{2-} \rfloor$ and $\lfloor Ba^{2+} \rfloor$ are, respectively the concentration in sulphate and barium and $K_s$ is the solubility of barium sulphate ($1.07 \times 10^{-10}\,mol^2\,l^{-2}$ at 22 °C).

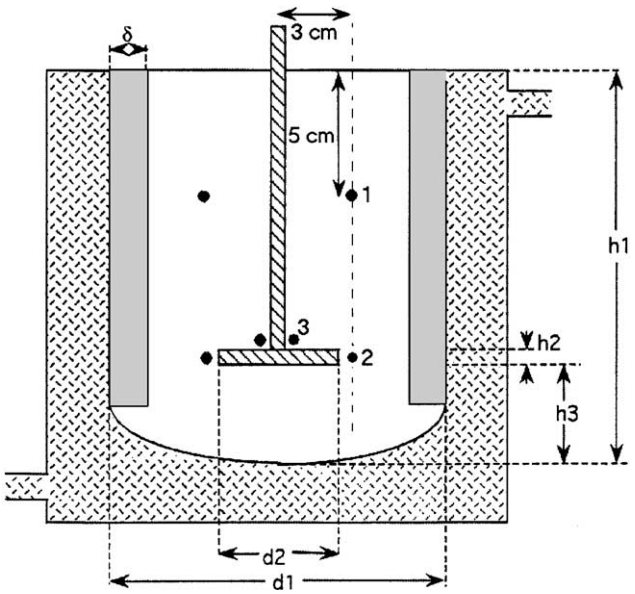


Fig. 1. Experimental set-up with the location of the feed points, $h_1$: total height of the reactive volume; $h_2$: thickness of the turbine; $h_3$: distance between the turbine and the vessel bottom; $d_1$: vessel inner diameter; $d_2$: turbine diameter; $\delta$: baffle width.

Table 1
Experimental conditions

| Experiment | Feed strategy | Feed rate (ml/h) | Feed time | Stirring (rpm) | Feed position |
|---|---|---|---|---|---|
| 1 | Double | 480 | 20 min | 500 | 1 |
| 1R | Double | 480 | 20 min | 500 | 1 |
| 2 | Single | 480 | 20 min | 500 | 1 |
| 3 | Double | 480 | 20 min | 1000 | 1 |
| 4 | Double | 480 | 20 mm | 250 | 1 |
| 5 | Double | 480 | 20 min | 250 | 2 |
| 6 | Double | 480 | 20 min | 250 | 3 |
| 7 | Double | 3840 | 2 min, 30 s | 500 | 1 |
| 8 | Single | 3840 | 2 min, 30 s | 500 | 1 |
| 9 | Double | 96 | 1 h, 40 min | 500 | 1 |
| 10 | Single | 96 | 1 h, 40 min | 500 | 1 |

Single and double jets experiments were conducted at several feed rates (Table 1).

At the end of each run, 1–2 $cm^3$ of the crystal suspension were carefully spread on a filtration membrane with the help of a peristaltic pump. After filtration and drying, a piece of the membrane was fixed on a support and gold-plated for examination by a scanning electron microscope (Jeol TM 330A, Jeol, Rueil–Malmaison, France). About 80 crystals per sample were analysed. Digital images on 256 grey levels were captured and transferred to a workstation on which the image analysis packages were implemented: Visilog™ 4.1.4 (Noesis, Les Ulis, France) and software developed in the laboratory.

### 2.2. Image analysis

A quick look to the different barium sulphate crystals described in literature as well as to those obtained during our experiments reveals that the particles differ from the point of view of their silhouette (bi-dimensional information) but also from the point of view of the roughness, related to twinning and stratified growth (tri-dimensional information). The calculated shape descriptors should be able to render both aspects.

Fig. 2 depicts the five main steps in the analysis of a barium sulphate crystal. The treatment of the initial grey level image (A) produces a binary image (C) which contains the particle silhouette. This transformation is obtained by enhancing the contour and any visible edge by delineation [19] of image (A) and by thresholding automatically the resulting image. Due to the presence of the filter, it is generally necessary for the operator to edit manually the image with a mouse to have a correct contourline (image (B)). Image (C) is obtained by hole-filling of image (B). The two other images ((D) and (E), respectively) of Fig. 2 show the convex bounding polygon ($H_c$), and the particle facets image, obtained by a logical combination of images (B) and (C).

The primary parameters computed on the particle silhouette (image (B)) are its surface $S$, from which the surface equivalent diameter $D_{eq} = 2\sqrt{S/\pi}$ is deduced, its Crofton perimeter $P$ [19], its Feret diameter distribution, from which the maximal diameter ($F_{max}$) (i.e. crystal "length") and minimal diameter ($F_{min}$) (i.e. crystal "width") are extracted. Dimensionless secondary parameters (circularity, $C = P^2/(4\pi S)$, and the elongation ratios $F_{max}/F_{min}$ and $F_{max}/D_{eq}$) are calculated. These descriptors characterise macroscopically the shape.

For a more detailed description, the silhouette is compared to its convex bounding polygon (image (D)). Let $\omega_1$ and $\omega_2$ be, respectively, the number of erosions necessary to eliminate completely the particle silhouette and its complement with respect to $H_c$ (of surface $S_c$). Two dimensionless shape descriptors are computed: $\Omega_1 = 2\omega_1/\sqrt{S}$ that characterises the particle robustness and $\Omega_2 = 2\omega_2/\sqrt{S}$ that is a measure of its largest concavity. A surface concavity index, $CI = S/S_c$, that quantifies globally the concavity of the object, is computed [20].

Finally a pseudo-3D parameter representing the complexity of the network of facets of the crystals is computed by determining the partition-in-squares: it is based on the distribution of squares inscribed in an object (in the case of the particle silhouette) or a set of objects (in the case of the particle facets) [21]. The principle is to divide the zones between edges (borderline, facet edges) into squares of increasing size, so that the total available area is covered. From the two distributions in number of the squares obtained on the facets and on the convex bounding polygon, a dimensionless simplicity ($\xi$) index is calculated. $\xi$ is equal to 1 for a particle without any facet.

### 2.3. Statistical tools

The comparison of two populations is based on three statistical tests: Student's *t*-test on means, Fisher's test on variances and Mann and Whitney's *U*-test on distribution shapes [22]. Different significance levels $\alpha$: are considered: if $\alpha > \alpha_s = 5\%$, the tested values (means, variances or distribution shapes) are not different, if $\alpha_s > \alpha > \alpha_1 = 1\%$, they are just different, if $\alpha_1 > \alpha > \alpha_2 = 0.5\%$, they are different, and if $\alpha < \alpha_2$, they are very different.

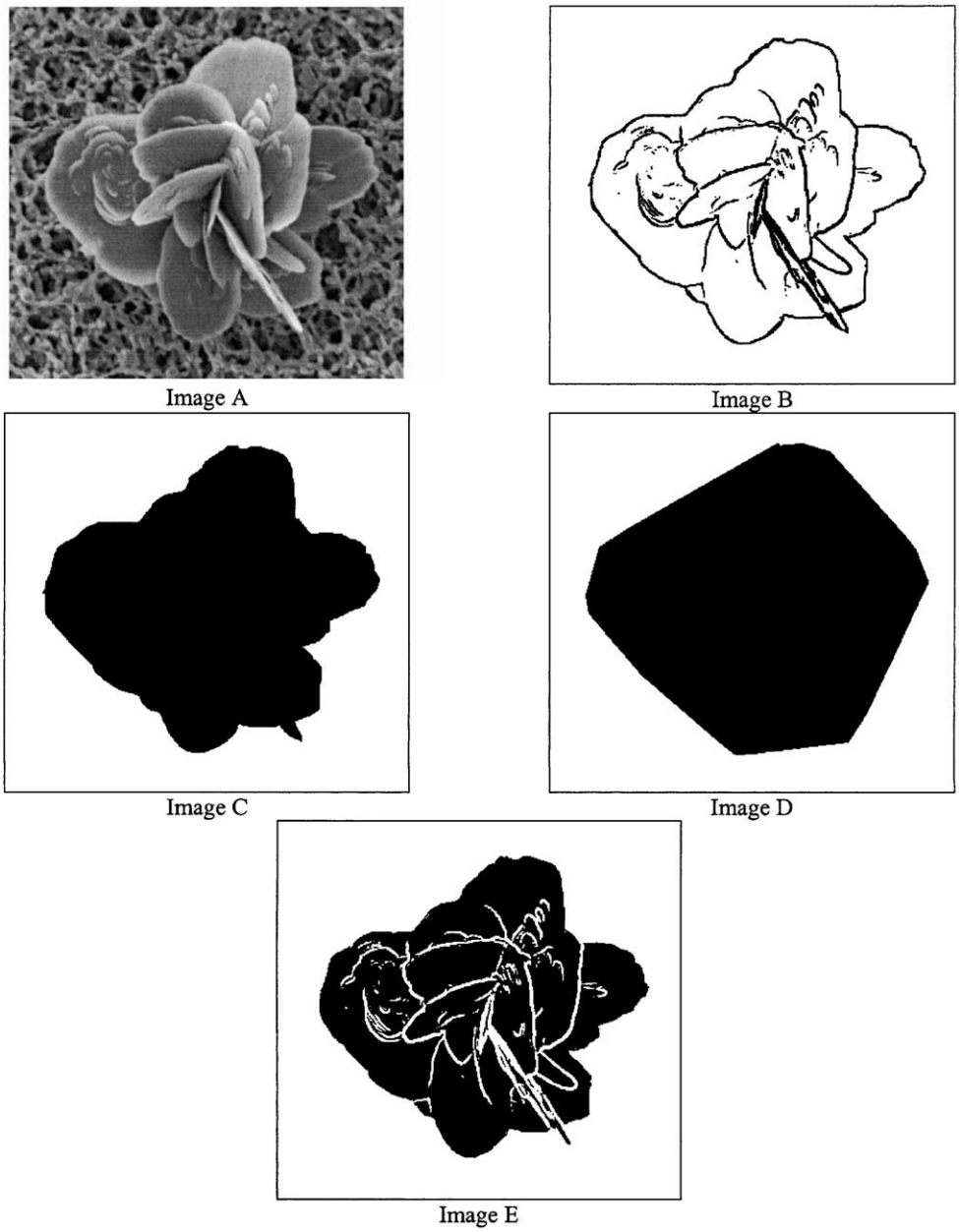


Fig. 2. The five main steps of the analysis of barium sulphate crystals micrographs.

To summarise the information carried by a set of descriptors it is useful to use a data-compressing technique such as principal component analysis [23]. Considering the original $(m, n)$-data matrix $\boldsymbol{X}$ with $n$ particles and $m$ descriptors, it is possible to reduce the dimension $m$ of the data set to a dimension $s < m$ with a minimum loss of information. Generally $s = 2$.

In the new space, $f_i = \sum_{j=1}^{m} a_{i,j} x_j$ for $i = 1$ to $s$. The Xlstat-toolbox for Excel (T. Fahmy, Paris, France) has been used for principal component analysis as well as for discriminant factorial analysis [23]: the later technique was employed for the automated classification of crystal according to their shape.

## 3. Results

### 3.1. Shape characterisation

The ability of the shape descriptors to discriminate between the different possible shapes of barium sulphate crystals has been first checked on literature data. Fischer and Rhinehammer [24] studied the effect of excess of potassium sulphate or barium chloride on the shape of crystals. Angerhöfer [25] investigated the change of habit in function of the relative supersaturation. In Fig. 3 the robustness $\Omega_1$ of the silhouettes of the crystals obtained by those authors has been plotted in function of the largest concavity index $\Omega_2$.

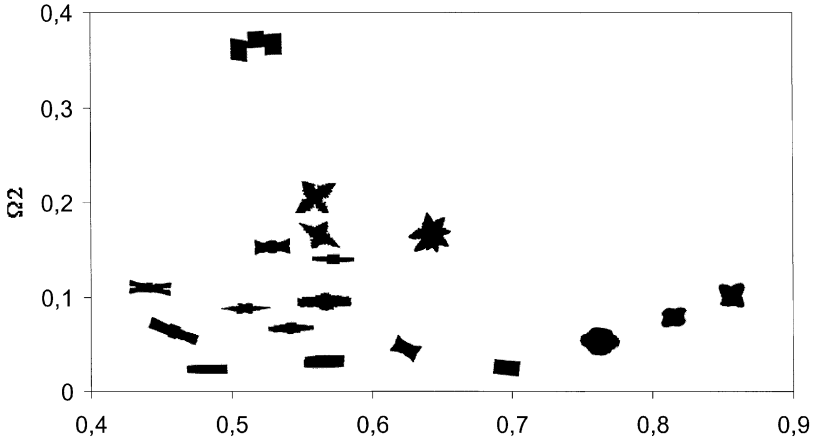


Fig. 3. Discrimination of crystals according to their robustness ($\Omega_1$) and largest concavity index ($\Omega_2$). Data from Fischer and Rhinehammer [24] and Angerhöfer [25].

The habits are well discriminated in function of their robustness and their concavity. A more precise discrimination can be obtained by considering the set of the six bi-dimensional descriptors: $F_{max}/F_{min}$, $F_{max}/D_{eq}$, $C$, CI, $\Omega_1$, $\Omega_2$. The quality of the photographs from literature was not good enough to be able to calculate the simplicity, which was therefore left out here. The first two principal components, $f_1$ and $f_2$, enable to represent 87% of the total variability of the observed habits. The circle of correlation, where the position of each descriptor in the $f_1$–$f_2$ space is plotted, reveals that each descriptor brings a significant information as all of them are well distributed on the circle (Fig. 4). In Fig. 5, compact crystals are on the left side of the graph and elongated ones on the right side. Convex shapes correspond to positive values of $f_2$ and concave ones to negative values.

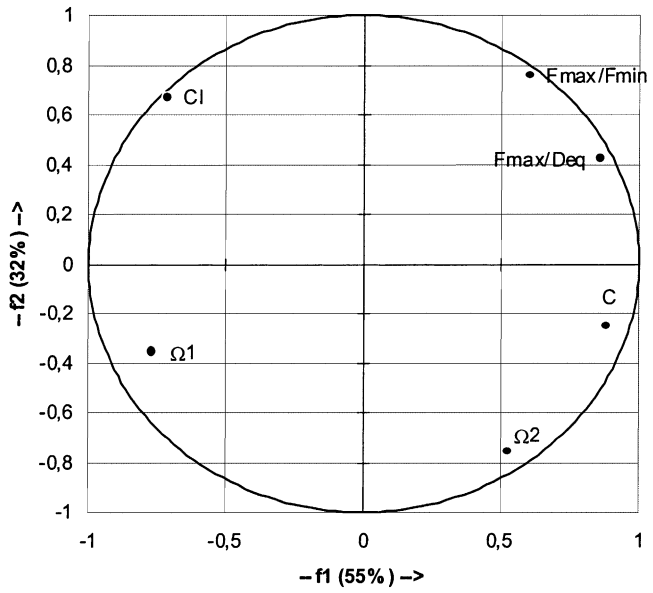


Fig. 4. Circle of correlation.

The surface roughness of the crystals, especially the quasi-rectangular ones, is easily quantified by the simplicity (Fig. 6).

### 3.2. Statistical validity

One of the difficulties in imaging small crystals such as those of barium sulphate is that the capture of scanning electron micrographs is time-consuming and that the sample preparation should be done very carefully to avoid partially occluding objects. It is therefore necessary to determine what is the minimal number of crystals to examine to obtain statistically valid results.

In studies on copper sulphate crystallisation [26] and calcium oxalate [18] it has been showed that, with a proper sampling method, 80 crystals were sufficient to statistically represent the particle population by meeting a hypothesis

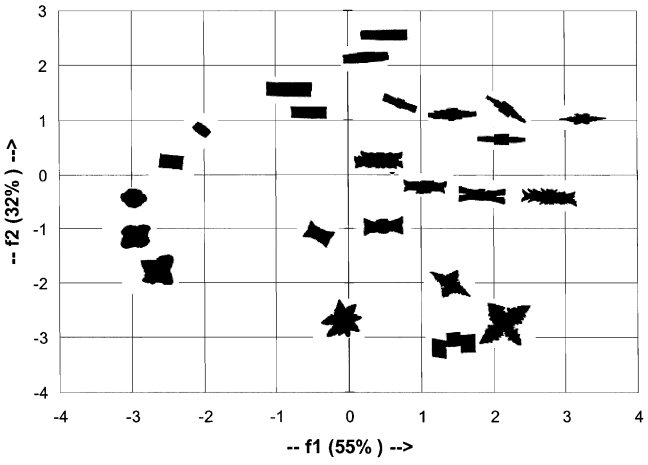


Fig. 5. Discrimination of crystals according to the shape of their silhouette in the plane $f_1$–$f_2$. Data from Fischer and Rhinehammer [24] and Angerhöfer [25].

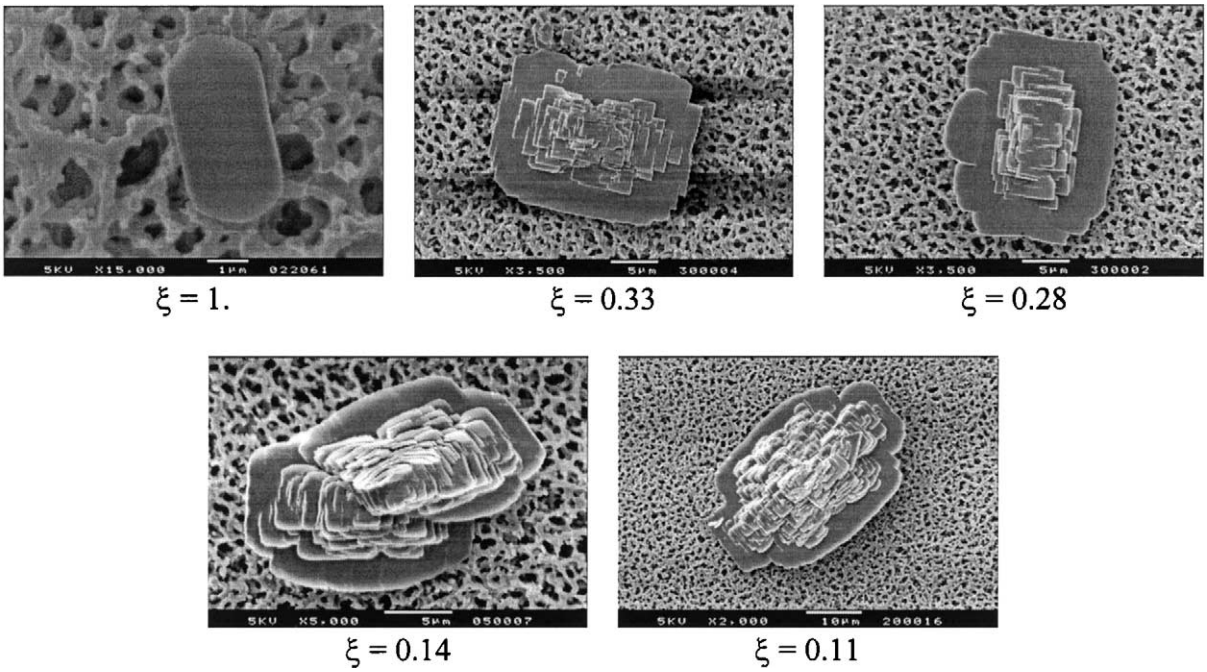


Fig. 6. Quantification of the degree of stratification by the simplicity descriptor—examples from different experiments

rejection criterion of 5%. By considering two sets of 80 particles from the same barium sulphate precipitation experiment, similar results were obtained for size and shape descriptors from the point of view of means and distribution shape.

Furthermore, experiment 1 (Table 1) was repeated: both runs were performed on the same day with the same aqueous solutions of reagents. Statistically similar populations in terms of size and bi-dimensional shape were obtained from the point of view of means, standard deviations and distribution shape ($\alpha > 5\%$). Despite the extreme care that was exercised to replicate the experiments exactly, there existed a difference in the stratification of platelets ($\alpha < 0.5\%$). A discrepancy was noticed for the simplicity parameter (Fig. 7),

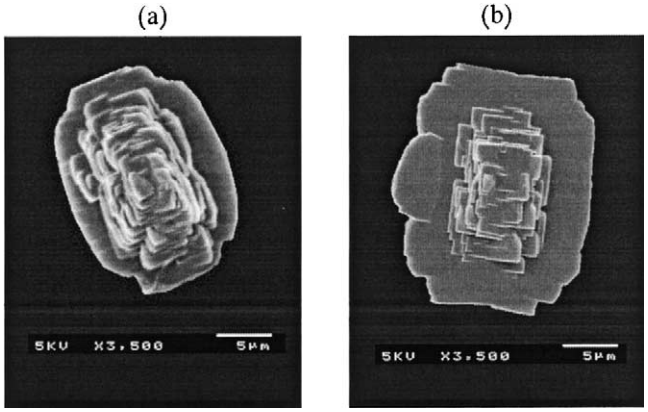


Fig. 7. Typical crystals obtained in run 1 (a) ($\xi = 0.33$) and its replication (b) ($\xi = 0.15$).

that corresponds to the visual aspect of the crystals, with higher simplicity ($\xi = 0.3$) obtained in the replication than in the initial run ($\xi = 0.15$). All the following results were obtained by examination of at least 80 crystals per run.

### 3.3. Global shape and size characterisation

Fig. 8a summarises in the space of the first two principal components, $f_1$ and $f_2$, the morphology distributions obtained for the different operational conditions of Table 1. For each experiment an average value of each shape descriptor is calculated. The principal component analysis was run on the average values of the following seven descriptors: $F_{max}/F_{min}$, $F_{max}/D_{eq}$, $C$, CI, $\Omega_1$, $\Omega_2$ and $\xi$. The 98% of the morphological information was summarised in the $f_1$–$f_2$ plane, with 85% for $f_1$ and 13% for $f_2$.

The $f_1$-axis corresponds to elongation and concavity information, while the $f_2$-axis corresponds mainly to the 3D information (simplicity). The positions of the points corresponding to runs 1 and 1R illustrate how the 3D-morphology of barium sulphate crystals is very sensitive to operating conditions.

From the point of view of size (Fig. 8b), two groups can be distinguished. The first one is composed of experiments 5, 7–9, with crystals of an average size of 16 μm. The second one is composed of experiments 1, 1R, 2–4, 6 and 10, and gives smaller crystals (9 μm). From the point of view of morphology (Fig. 8a), two other groups can also be distinguished. The first one is composed of experiments 6, 8–10, where elongated crystals with large concavities

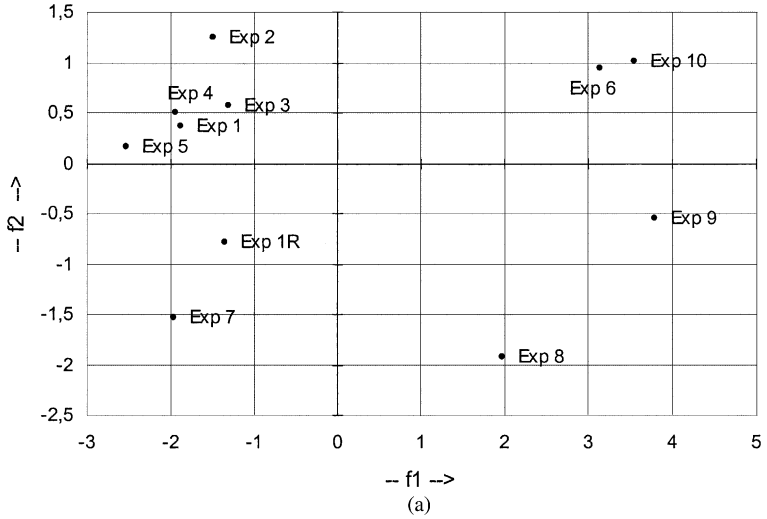


(a)

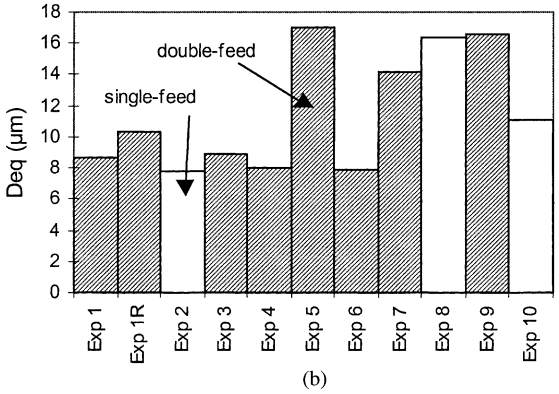


(b)

Fig. 8. Global assessment of the effect of operational conditions on shape (a) and size (b) of barium sulphate crystals.

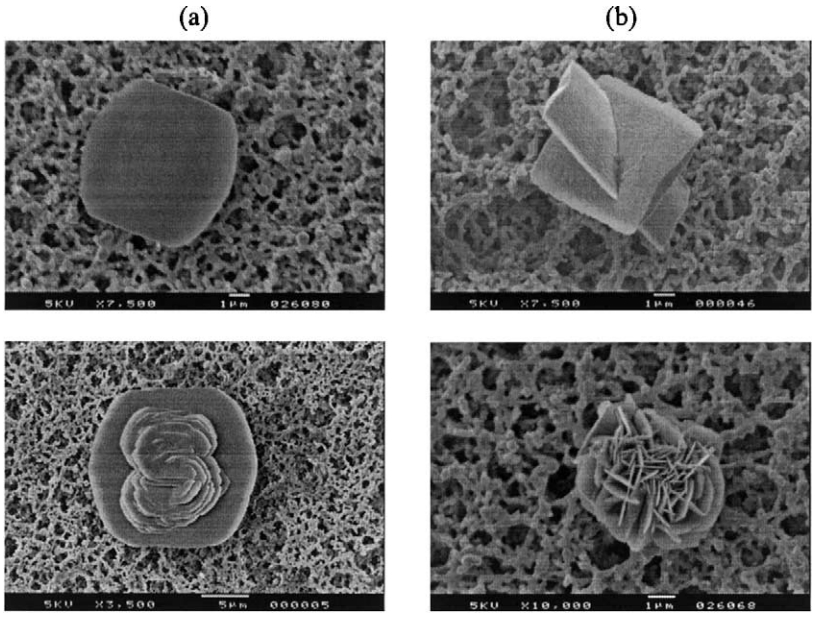


Fig. 9. Shape classes: platelets (a) and sand-roses (b)

Table 2
Reference shape descriptors of platelets and sand-roses used for classification[a]

| | $F_{max}/F_{min}$ | $F_{max}/D_{eq}$ | $C$ | CI | $\Omega_1$ | $\Omega_2$ |
|---|---|---|---|---|---|---|
| Platelets | 1.38 (0.39) | 1.18 (0.15) | 1.17 (0.17) | 0.01 (0.02) | 0.75 (0.02) | 0.03 (0.08) |
| Sand-roses | 1.34 (0.21) | 1.22 (0.10) | 1.45 (0.40) | 0.08 (0.07) | 0.71 (0.08) | 0.1 (0.05) |

[a] The standard deviation of the training subsets are given in parentheses.

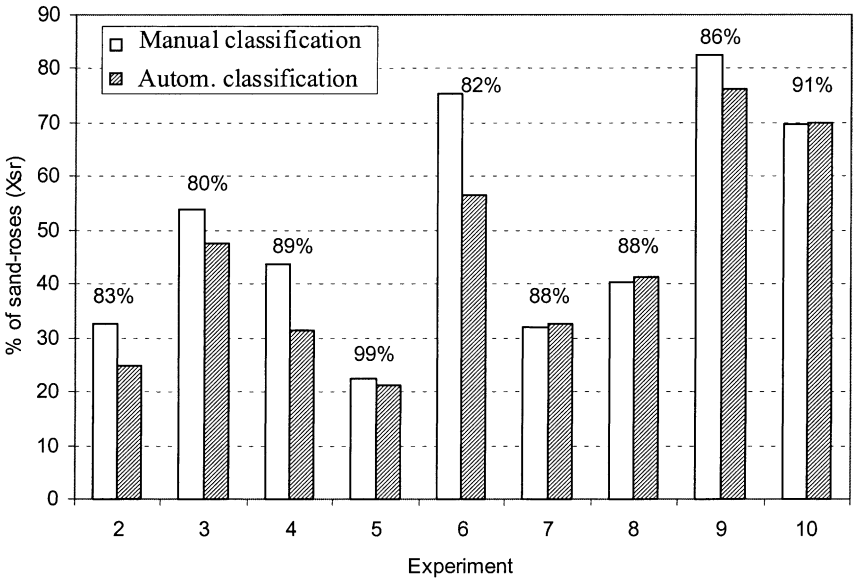


Fig. 10. Comparison of the manual and automated classification of crystals according to their shape with the percentage of well-classified crystals.

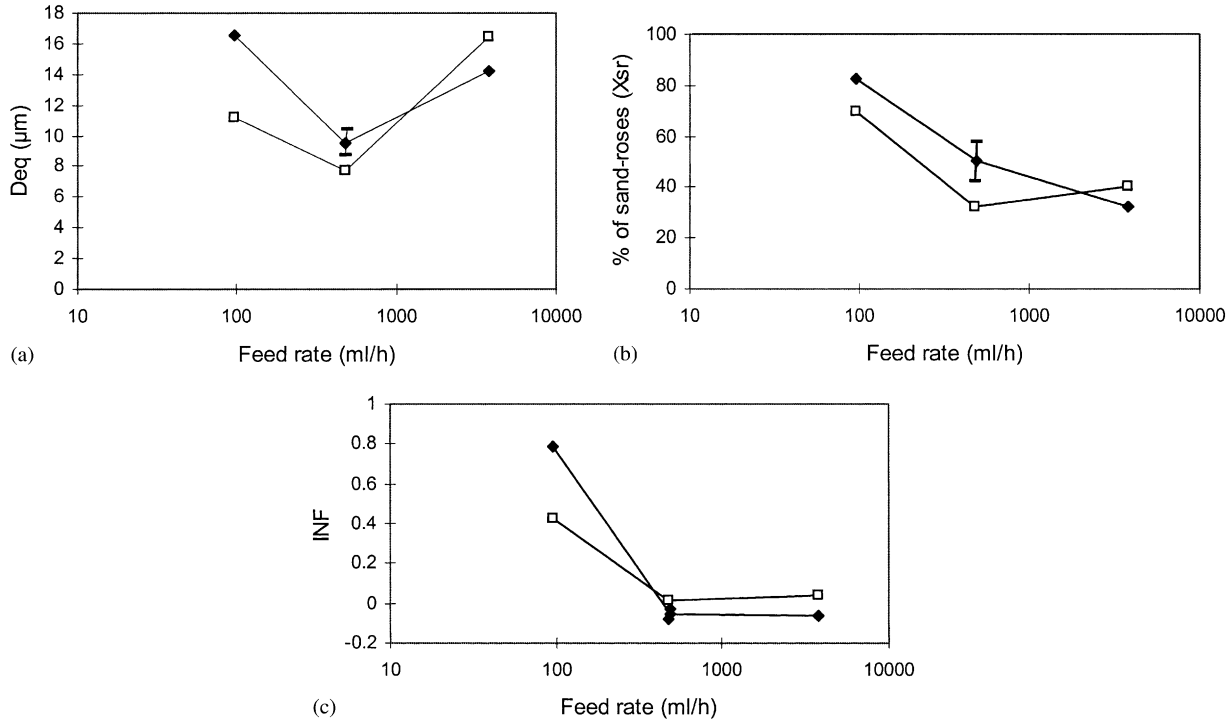


Fig. 11. Effect of the operational conditions on the average crystal size (a); the proportion of sand-roses, $X_{sr}$ (b) and the influence factor INF (c). (□) Single feed; (◆) double feed.

are prevalent. The second one is composed of experiments 1, 1R, 2–5 and 7, with predominantly, more compact crystals.

Taking into consideration the information on both size and shape, experiments 5 and 9 produced crystals with similar size (about 16 μm), but different shapes. Experiment 6 produces crystals with same size (about 8 μm) than experiments 1–4, but with different shapes: it gives more elongated and concave crystals than the other experiments.

Stirring speed has no effect on average size and shape of crystals (experiments 1, 1R, 3 and 4). Feed position (experiment 4–6) has an influence both on size (larger crystals are obtained in experiment 5) and shape (more irregular crystals are obtained in experiment 6). Single or double feed strategy has an effect on shape only for very high feed rates (experiments 7 and 8) and an effect on size only for very low feed rate (experiments 9 and 10). Feed rate has an effect both on size and shape for single (experiments 10, 2 and 8) or double (experiments 9, 1 and 7) feed strategies.

### 3.4. Detailed size and shape characterisation

#### 3.4.1. FDA analysis and classification

A more detailed characterisation can be done by defining shape classes and examining how the fraction of crystals belonging to each class changes in function of the operational conditions. Once the shape classes have been defined, discriminant factorial analysis offers a statistical method for the classification of crystals [23]. It is based on establishing a relationship between a qualitative variable (e.g. the shape or class) describing an object and a number of quantitative parameters (e.g. the morphological parameters) calculated on the object.

All the barium sulphate particles produced in the experiments can be classified into two morphological groups: platelets and sand-roses (Fig. 9). The bi-dimensional shape descriptors were used for the classification and the average values for the two shape classes are given in Table 2. A set of 300 particles, from runs 1 and 1R, was selected for training. In the validation step performed on the crystals obtained

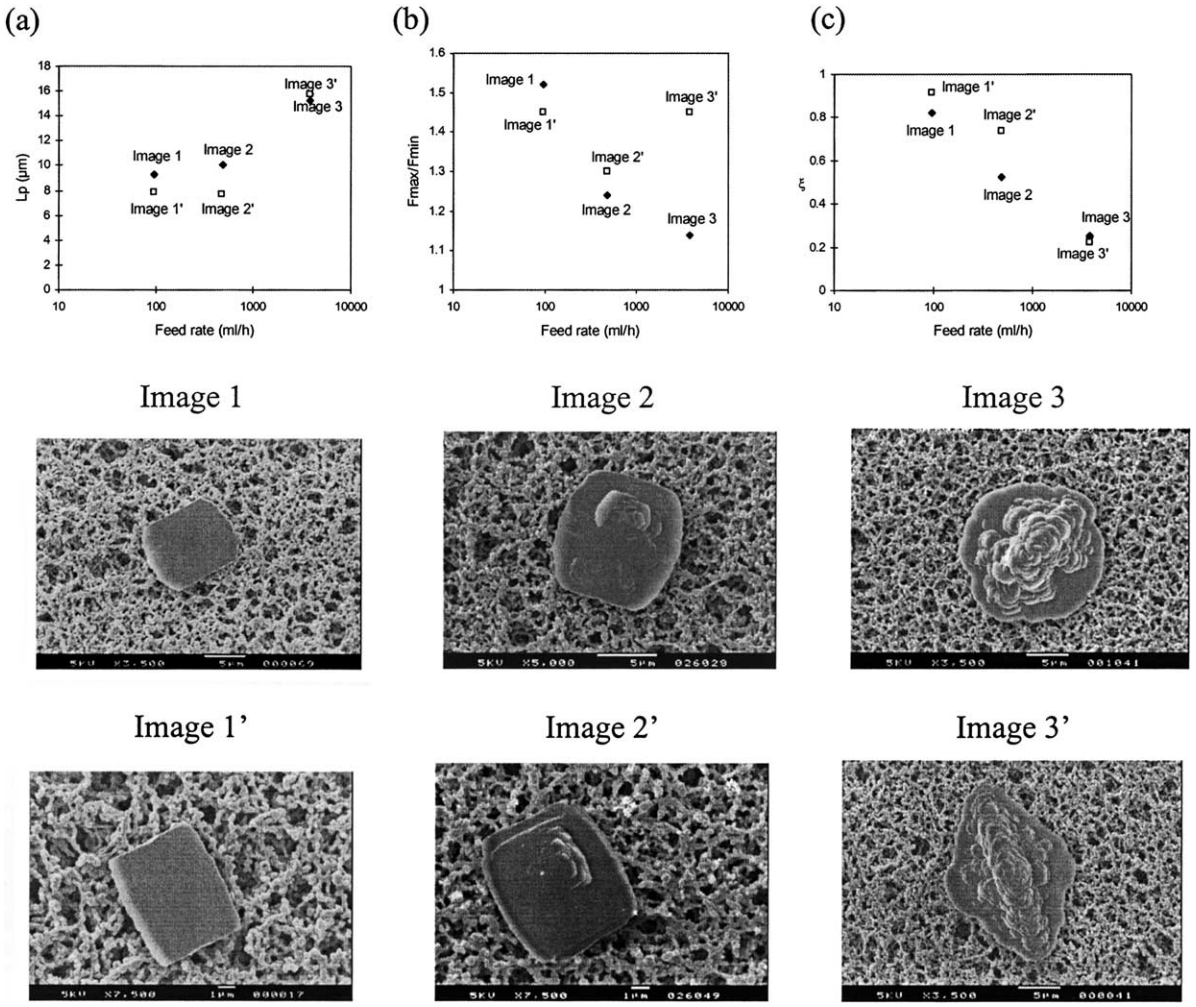


Fig. 12. Effect of the operational conditions on the size (a), the elongation (b) and the simplicity (c) of platelets with some typical crystals. (□) Single feed; (◆) double feed.

in the other experiments, the rate of success was larger than 80%. Fig. 10 summarises the proportion of sand-roses ($X_{sr}$) found by manual and automated classifications for all the experiments, except those used for training.

*3.4.2. Influence factor analysis*

To describe the effect of the shape on the size distribution in each run, the average equivalent diameters of platelets ($L_p$) and sand-roses ($L_{sr}$) are calculated. $\bar{L}$ is the average size of the crystal population and can be written as:

$$\bar{L} = X_{sr}L_{sr} + (1 - X_{sr})L_p$$

that can be rewritten as:

$$\bar{L} = (1 + \mathrm{INF})L_p$$

where the influence factor 'INF' is defined as $\mathrm{INF} = X_{sr}(L_{sr} - L_p)/L_p$.

This formalism is similar to the one used by Bernard-Michel et al. [18] for calcium oxalate precipitation.

Independently from the injection type, $\bar{L}$ varies with the feed rate and a minimal value is observed for an intermediate feed rate (Fig. 11a). The proportion of sand-roses (Fig. 11b) decreases as well as their influence (Fig. 11c) on the crystal population average size when the feed rate increases.

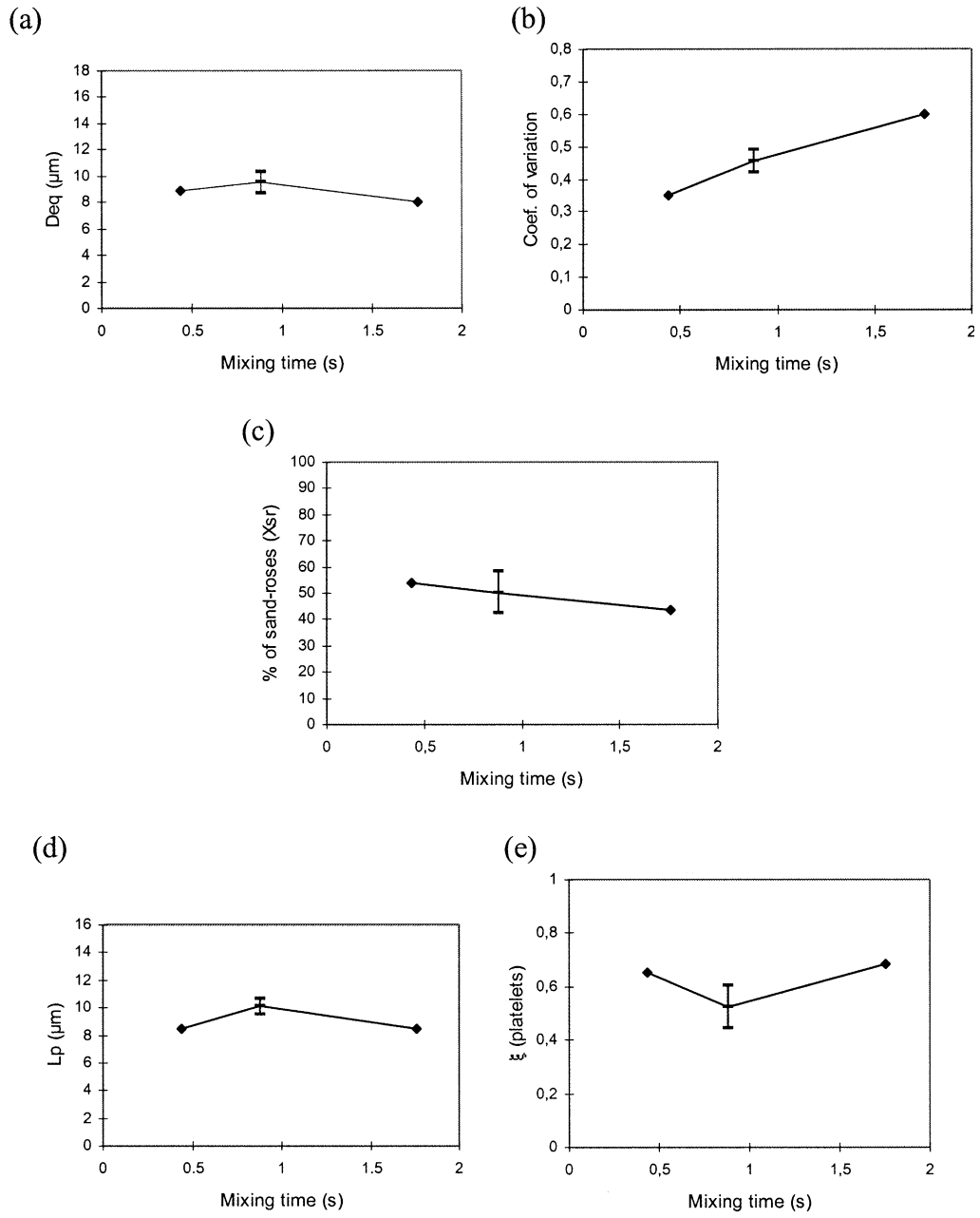


Fig. 13. Effect of macromixing on size and morphology: average size of crystals (a) and coefficient of variation of the size distribution (b); percentage of sand-roses (c); size (d) and simplicity (e) of platelets.

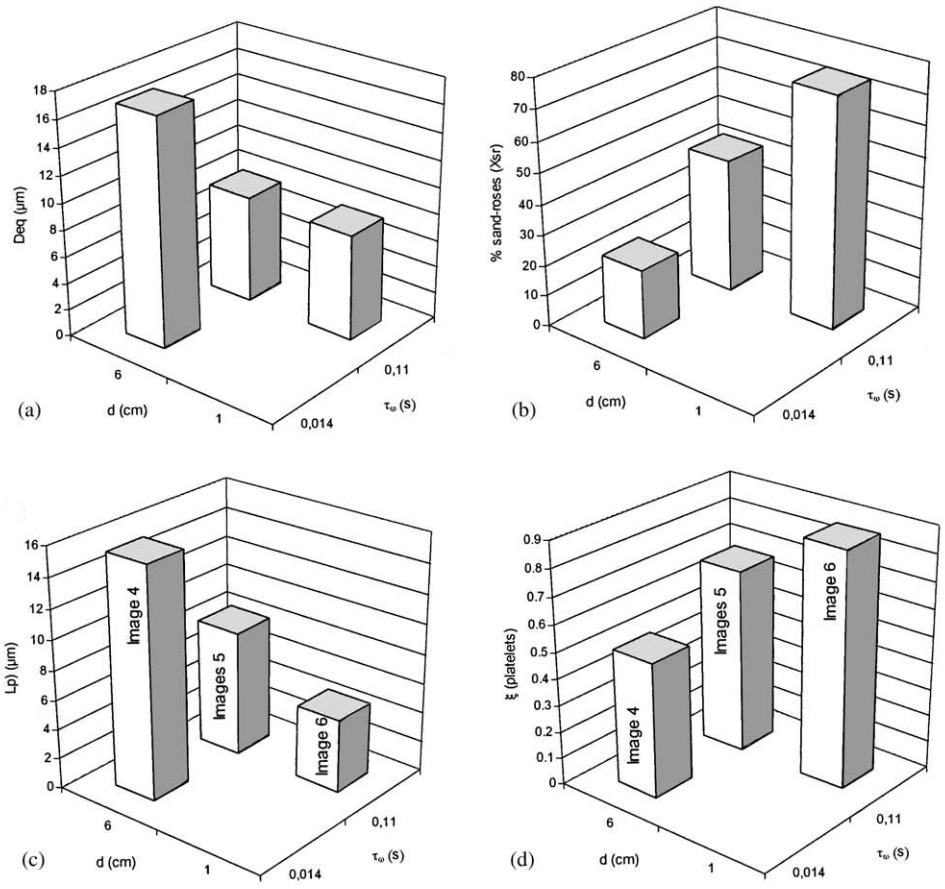


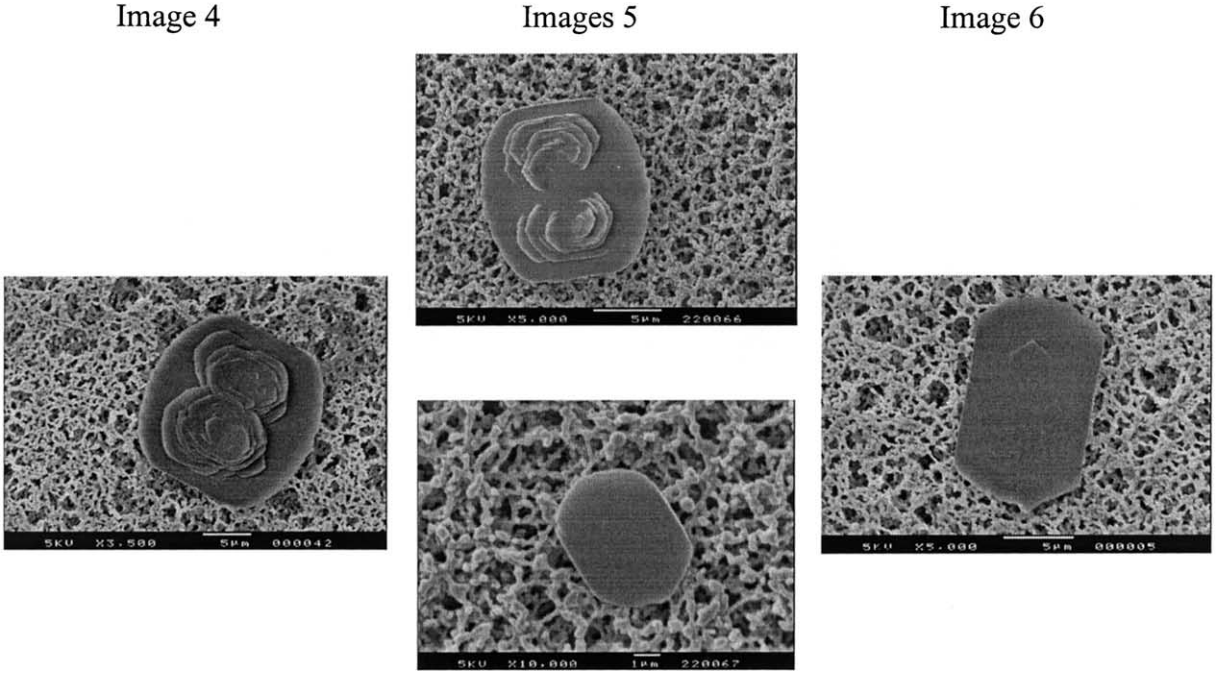


Fig. 14. Effect of micromixing on size and morphology: average size of crystals (a); percentage of sand-roses (b), size (c) and simplicity (d) of platelets with some typical platelets.

*3.4.3. 2D and pseudo-3D analysis*

From the point of view of size (Fig. 12), for each feed rate, double and single feed strategies yield to platelets quite similar. Double and single feed strategies yield to platelets that differ by their elongation only for high feed flow rates (Fig. 12b), with single feed giving more elongated platelets than double feed. Size (Fig. 12a) and stratification (Fig. 12c) of platelets increase when the feed flow rate increases. Their elongation decreases when the feed flow rate increases in the case of the double feed strategy. Fig. 12 contains also some typical images of the most predominant crystal shape.

*3.5. Effect of macro and micromixing*

*3.5.1. Macromixing analysis*

The circulation time corresponds to the time necessary for the recycle of a fluid element. This parameter represents the macromixing in the reactor. For a continuous stirred-tank crystalliser equipped with a Rushton turbine, the circulation time is defined as:

$$t_c = 0.85\frac{(T/D)^2}{N}$$

where $T$ is the reactor diameter, $D$ the diameter of the turbine and $N$ the stirring speed.

The experiments 4, 1, 1R and 3 were performed with increased stirring speed, all the other operational parameters being kept constant. The average size $\bar{L}$ is almost unaffected by the mixing time (Fig. 13a). The coefficient of variation of the size distribution (100 × standard deviation/average) increases with $t_c$ (Fig. 13b). The proportions of platelets and sand-roses is such that the global size distribution is bimodal; the percentage of sand-roses decreases slightly (Fig. 13c) when $t_c$ increases. The shape of platelets is not affected by the mixing time: $D_{eq} \approx 9\,\mu m$, $F_{max}/F_{min} \approx 1.2$, $\xi \approx 0.5$–$0.6$ (Fig. 13d and e).

*3.5.2. Micromixing analysis*

Baldyga and Bourne [27] represent the mixing mechanism at molecular scale (micromixing) by the engulfment of a fluid element in another, creating then a vortex dissipating energy and having a life time $\tau_w$ given by:

$$\tau_w = 12\left(\frac{\nu}{\varepsilon}\right)^{1/2}$$

where $\nu$ is the kinematic viscosity ($10^{-6}\,m^2\,s^{-1}$) and $\varepsilon$ is local energy dissipation rate [27].

David and Marcant [28] predicted micromixing effects in the case of a double feed precipitation. The model has two key parameters: one represents the local turbulence level that is characterised by the micromixing time $\tau_w$ in the feed area, and the second one represents the interaction between the two jets and is characterised by the distance $d$ between these two jets.

The platelets shown in Fig. 14 are typical of those collected during the experiments 4–6. Small sand-roses are predominantly formed when $\tau_w$ is large (Fig. 14b), when $d$ decreases, the size (Fig. 14c) and stratification of the platelets decrease as the simplicity increases (Fig. 14d), but they are more elongated (platelets 5 and 6). when $\tau_w$ decreases, the size and stratification of platelets increase as $\xi$ decreases slightly, and elongation is constant (platelets 4 and 5).

## 4. Conclusions

The size and morphology of barium sulphate crystals obtained under different operational conditions has been quantitatively assessed by image analysis. Six descriptors are used to characterise the projected silhouette of each imaged particle. In the specific case of barium sulphate crystals, the extent of stratified growth is measured via a pseudo-3D descriptor.

The results of the present investigation shows that tools providing this information for sets of particles are available if some care is used for the sample preparation. This information can be valuably used to introduce, in greater details than what is done actually, morphology in the modelling of precipitation and crystallisation processes. Many problems remain open, such as how to bridge the gaps between crystal molecular simulation, morphology description of a crystal population and powder end-use properties.

## References

[1] D.J. Gunn, M.S. Murthy, Kinetics and mechanisms of precipitation, Chem. Eng. Sci. 27 (1972) 1293–1313.
[2] M.S. Murthy, Theory of crystal growth in phase transformations: precipitation of barium sulphate, Chem. Eng. Sci. 49 (1994) 2389–2393.
[3] J. Hostomsky, A.G. Jones, Crystallization and agglomeration kinetics of calcium carbonate and barium sulphate in the MSMPR crystallizer, in: Proceedings of the 12th Symposium on Industrial Crystallization, Vol. 1, Warsaw, 1993, pp. 49–54.
[4] M. Angerhöfer, A. Mersmann, Determination of nucleation and growth kinetics from batch precipitation of barium sulphate, in: Proceedings of the 12th Symposium on Industrial Crystallization, Vol. 1, Warsaw, 1993, pp. 61–66.
[5] S. Kipp, R. Lacmann, M. Reichelt, W. Schröder, Tailor-made additives to influence the habit of barite ($BaSO_4$) obtained by precipitation, Chem. Eng. Technol. 19 (1996) 543–549.
[6] M. Aoun, Etude cinétique par une nouvelle méthode de la précipitation du sulfate de baryum à partir de différentes solutions réactives et à stoechiométrie variable, Ph.D. Thesis, Institut National Polytechnique de Lorraine, Nancy, France, 1996.
[7] R. Mohanty, Bhandarkar, Zuromski, R. Brown, J. Estrin, Characterizing the product crystals from a mixing tee process, AIChE J. 34 (1988) 2063–2068.
[8] D.E. Fitchett, J.M. Tarbell, Effect of mixing on the precipitation of barium sulfate in an MSMPR reactor, AIChE J. 36 (1990) 511–522.
[9] T. Meyer, P.A. Fleury, A. Renken, J. Darbellay, P. Larpin, Barium sulfate precipitation as model reaction for segregation studies at pilot scale, Chem. Eng. Proc. 31 (1992) 307–310.
[10] J. Baldyga, W. Podgorska, R. Pohorecki, Mixing-precipitation model with application to double feed semi-batch precipitation, Chem. Eng. Sci. 50 (1995) 1281–1300.

[11] R. Philips, S. Rohani, J. Baldyga, Micromixing in a single-feed semi-batch precipitation process, AIChE J. 45 (1999) 82–92.
[12] M.L.J. van Leuwen, O.S.L. Bruinsma, G.M. van Rosmalen, Precipitation and mixing: influence of hydrodynamics on crystal size and shape, in: Proceedings of the 5th World Congress on Chemical Engineering, Vol. 5, San Diego, CA, 1996, pp. 710–715.
[13] P. Pénicot, H. Muhr, E. Plasari, J. Villermaux, Influence of the internal crystallizer geometry and the operational conditions on the solid product quality, Chem. Eng. Technol. 21 (1998) 507–514.
[14] P. Bowen, R. Humphry-Baker, P. Eriksson, C. Hérard, Submicron particle size distribution (PSD) measurement using the Horiba CAPA-700 and preliminary studies on the PSD measurement of anisotropic particles, in: Proceedings of the 5th World Congress on Chemical Engineering, Vol. 6, San Diego, CA, 1996, pp. 518–523.
[15] M. Naito, O. Hayakawa, K. Nakahira, H. Mori, J. Tsubaki, Effect of particle shape on the particle size distribution measured with commercial equipment, Powder Technol. 100 (1998) 52–60.
[16] F. Trdic, J. Strazisar, A. Vrhunec, I. Livk, C. Pohar, Determination of crystal size distribution by using image processing technology, in: Proceedings of the 13th Symposium on Industrial Crystallization, Vol. 2, Toulouse, France, 1996, pp. 833–838.
[17] M.N. Pons, H. Vivier, K. Belaroui, B. Bernard-Michel, F. Cordier, D. Oulhana, J. Dodds, Particle morphology: from visualisation to measurement, Powder Technol. 103 (1999) 44–57.
[18] B. Bernard-Michel, M.N. Pons, H. Vivier, S. Rohani, The study of calcium oxalate precipitation using image analysis, Chem. Eng. J. 75 (1999) 93–103.
[19] J.C. Russ, The Image Processing Handbook, 2nd Edition, CRC Press, Boca Raton, 1995.
[20] M.N. Pons, H. Vivier, J. Dodds, Particle shape characterization using morphological descriptors, Part. Syst. Charact. 14 (1997) 272–277.
[21] M.N. Pons, H. Vivier, T. Rolland, Pseudo-3D shape description for facetted materials, Part. Syst. Charact. 15 (1998) 100–107.
[22] Wodsworth, Handbook of Statistical Methods for Engineers and Scientists, McGraw Hill, New York, 1990.
[23] J.W. Einax, H.W. Zwanziger, S. Geiß, Chemometrics in Environmental Analysis, VCH, Munich, 1997.
[24] R.B. Fischer, T.B. Rhinehammer, Rapid precipitation of barium sulfate, Anal. Chem. 25 (1953) 1544–1548.
[25] M. Angerhöfer, Untersuchungen zur Kinetik der Fällungskristallisation von Bariumsulfat, Ph.D thesis, Technischen Universität München, Munich, Germany, 1994.
[26] B. Bernard-Michel, D. Jeanjean, M.N. Pons, H. Muhr, H. Vivier, J.L. Houzelot, Influence des paramètres opératoires sur la morphologie des cristaux, Récents Progrès Génie Procédés 11 (54) (1997) 171–176.
[27] J. Baldyga, J.R. Bourne, Calculation of micromixing in inhomogenous stirred tank reactors, Chem. Eng. Res. Dev. 66 (1988) 33–38.
[28] R. David, B. Marcant, Prediction of micromixing effects in precipitation: case of double-jet precipitators, AIChE J. 40 (1994) 424–432.